

Polar self-organization of ferroelectric nematic liquid crystal molecules on atomically flat Au(111) surface

Alexandr A. Marchenko^{1,2}, Oleksiy L. Kapitanchuk³, Yaroslava Yu. Lopatina^{1,2}, Kostiantyn G. Nazarenko^{4,5}, Anton I. Senenko¹, Nathalie Katsonis², Vassili G. Nazarenko^{1,6}, and Oleg D. Lavrentovich⁷

¹*Institute of Physics of the National Academy of Sciences of Ukraine, 46 Nauki ave., Kyiv, 03028, Ukraine*

²*Stratingh Institute for Chemistry, University of Groningen, Nijenborgh 4, 9747AG Groningen, The Netherlands*

³*Bogolyubov Institute for Theoretical Physics of the National Academy of Sciences of Ukraine, 14-B Metrologichna str., Kyiv, 03143, Ukraine*

⁴*Institute of Organic Chemistry of the National Academy of Sciences of Ukraine, Kyiv, Ukraine;*

⁵*Enamine Ltd, Kyiv, Ukraine*

⁶*Institute of Physical Chemistry, PAS, Kasprzaka 44/52, 01-224 Warsaw, Poland*

⁷*Advanced Materials and Liquid Crystal Institute, Department of Physics, Materials Science Graduate Program, Kent State University, Kent, OH 44242, USA.*

Abstract

Understanding nanoscale mechanisms responsible for the recently discovered ferroelectric nematics can be helped by direct visualization of self-assembly of strongly polar molecules. Here we report on scanning tunneling microscopy (STM) studies of monomolecular layers of a ferroelectric nematic liquid crystal on a reconstructed Au(111) surface. The monolayers are obtained by deposition from a solution at ambient conditions. The adsorbed ferroelectric nematic molecules self-assemble into regular rows with tilted orientation, resembling a layered structure of a smectic C. Remarkably, each molecular dipole in this architecture is oriented along the same direction giving rise to polar ferroelectric ordering.

Introduction

The simplest example of an orientationally ordered liquid is a uniaxial paraelectric nematic (N) liquid crystal (LC). The average orientation of molecules in the N phase is described by a unit vector $\hat{\mathbf{n}}$, called the director. The states $\hat{\mathbf{n}}$ and $-\hat{\mathbf{n}}$ are equivalent since the order is apolar, with no distinction between heads and ends of the rod-like molecules [1]. Recent discoveries [2-6] revealed a new ferroelectric nematic (N_F) phase with the polar orientation of molecules carrying large dipole moments, about 9-10 D, which is 1.5-2 times stronger than the dipole moments of many conventional N mesogens. Unidirectional alignment of dipoles yields spontaneous macroscopic electric polarization \mathbf{P} , locally parallel to the director $\hat{\mathbf{n}} \equiv -\hat{\mathbf{n}}$. The large polarization enables strong polarity-sensitive linear coupling to an applied electric field. Molecular orientation in an N_F slab could be realigned by electric fields on the order of $\sim 10^2$ V/m, thousand times smaller than those used to reorient conventional Ns [6].

The observation of N_F has been followed by the discovery of an antiferroelectric smectic SmZ_A with \mathbf{P} parallel to equidistant layers [7] and ferroelectric smectic A (SmA_F), in which the molecules form layers perpendicular to \mathbf{P} [8,9]. Besides stronger dipole moments, the N_F , SmZ_A , and SmA_F molecules are otherwise similar to the molecules forming the paraelectric N. The N_F , SmZ_A , and SmA_F phases readily transform into the N upon minute changes in temperature or as a result of a single-atom replacement in the molecules. The nanoscale underpinning of this delicate balance is far from being understood. The picture is certainly far more complex than a simple electrostatic concept that two parallel dipoles attract when placed head-to-tail and repel when placed side-by-side. Direct experimental visualization of self-organization of polar molecules could provide insight into the mechanisms. This work presents such a visualization, enabled by scanning tunneling microscopy (STM) of two-dimensional monolayers at atomically flat crystal substrates, Fig.1.

Interactions with bounding substrates are known to affect ferroelectric nematics strongly [6,10,11]. The polarization \mathbf{P} could be aligned by confining the material between two glass plates with unidirectionally rubbed polymer coatings [5-19]. Alignment of the N_F at solid crystalline substrates is studied much less. It is not clear

whether **P** will be aligned by a crystal substrate with well-defined crystallographic axes but no in-plane polar direction.

To visualize ferroelectric nematic molecules, we explore self-assembled monolayers (SAMs) of the N_F material 2,3',4',5'-tetrafluorobiphenyl-4yl 2,6-difluoro-4-(5-propyl-1,3-dioxan-2-yl)benzoate (also known as DIO [2]), Fig.1b (inset), adsorbed at an atomically flat reconstructed Au (111) substrate. STM reveals the polar orientation of the N_F molecules in the monolayer. These arrangements are in striking contrast to non-polar alignment in monolayers of the N mesogen 4-n-decyl-4'-cyanobiphenyl (10CB), Fig.1d (inset), at the same experimental conditions.

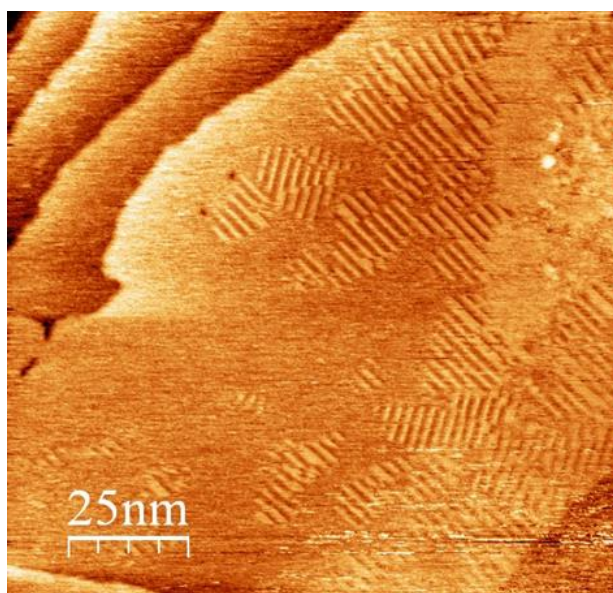
Materials and methods

The reconstructed Au(111) substrates are prepared from gold films deposited in ultra-high vacuum ($\sim 5 \times 10^{-8}$ Pa) onto a freshly cleaved mica heated to ~ 600 K, followed by annealing in a propane-air flame. On cooling from the isotropic (I) phase, the phase sequence of DIO is I–174°C –N–82°C –SmZ_A–66°C –N_F–34°C –Crystal, where SmZ_A is an antiferroelectric smectic with a partial splay [2,9,20]. At solid substrates, the DIO molecules and thus **P** align parallel to the substrate, to avoid a strong surface charge [10,18,21-26]. DIO is dissolved in tetradecane (99% purity, Aldrich), to a concentration of approximately ~ 0.05 mg/ml. The droplet of the DIO solution is placed onto the Au(111) substrate. Atomic-level imaging is performed with a PicoSPM from Molecular Imaging (USA) at ambient conditions. The STM tip is a Pt/Ir (80:20) wire sharpened by mechanical cutting. Typical imaging conditions correspond to a bias voltage U_t in the range 50-500 mV and a tunneling current $I_t = 50$ -500 pA. The error of measured distances is within 5%. Several STM images in the constant-current mode are recorded with different samples and tips to verify reproducibility. Film preparation and STM imaging are performed at room temperature ($\sim 20^\circ\text{C}$).

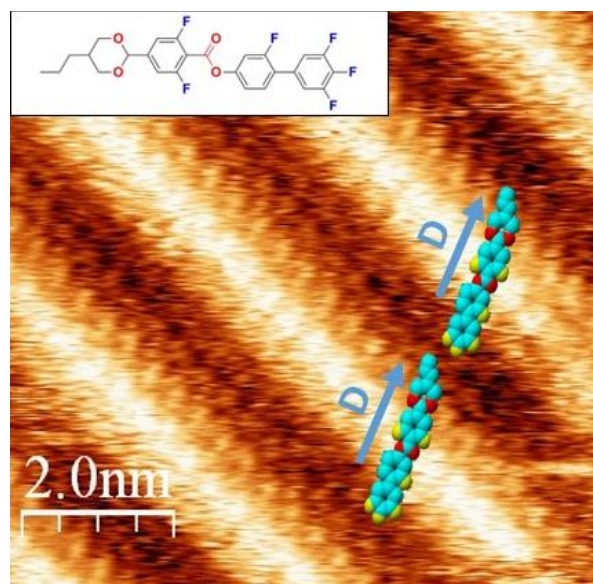
Results and discussion

Figure 1a shows the large-scale STM image of the N_F film at the Au(111) substrate at ambient conditions. The molecules form well-ordered bright layers. The layers tend to be perpendicular to the atomic step edges of the Au(111) substrate, as seen in the top

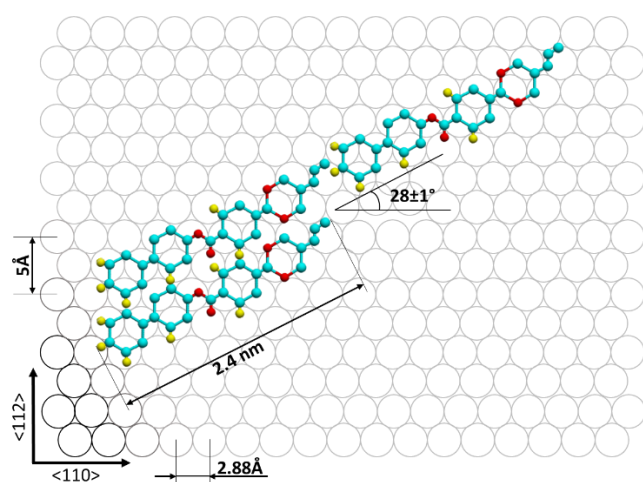
right corner of Fig. 1a. Since the step edges of Au(111) surface are parallel to the crystallographic $\langle 110 \rangle$ direction [27,28] one concludes that molecular layers are stacked along the perpendicular $\langle 11\bar{2} \rangle$ direction. The layers in neighboring domains make angles $60^\circ \pm 5^\circ$ or $120^\circ \pm 5^\circ$ with each other that correspond to the angle between the equivalent crystallographic $\langle 110 \rangle$, $\langle 101 \rangle$ and $\langle 011 \rangle$ directions of Au(111) surface.



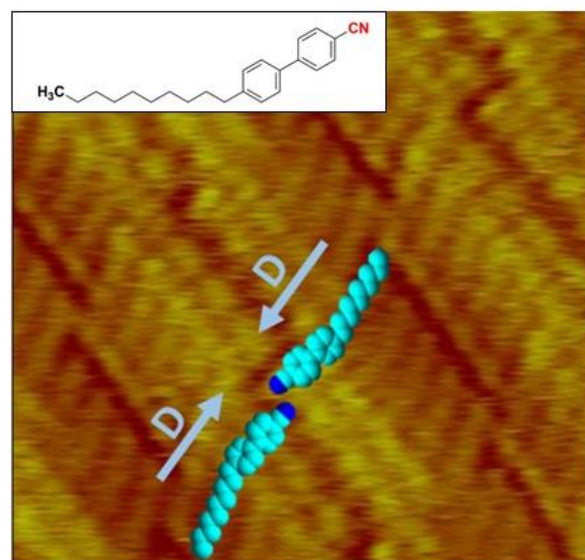
a



b



c



d

Figure 1. a) Large-scale STM image of a monomolecular DIO film on Au(111) surface. $I_t = 200$ pA, $U_t = 250$ mV. b) High-resolution image of adsorbed DIO molecules. The schematic position of adsorbed molecules is illustrated with a model

drawing. The molecular dipoles \mathbf{D} align unidirectionally. $I_t = 200$ pA, $U_t = 250$ mV. c) Schematic arrangement of DIO molecules on Au(111) surface with the optimized energy of interaction with the Au lattice. d) Self-organized monolayer of mesogenic 10CB molecules on Au(111) surface with a head-to-head packing. $I_t = 300$ pA, $U_t = 300$ mV.

The STM image in Fig. 1b resolves individual DIO molecules within the layers. Conjugated π -electron systems are known to provide a strong STM contrast [29,30], thus the bright region within each molecule can be identified with its aromatic core. Darker regions represent lower electron density associated with alkyl chains. From Fig. 1b, the molecular length is estimated as $l = (24.0 \pm 0.2)$ Å, and the side-by-side molecular separation as $w = (4.4 \pm 0.2)$ Å, somewhat larger than 4.2 Å reported for the bulk DIO in the SmZ_A phase [7]. The larger separation w is expected since the molecules lie flat at the substrate. The width of a molecular row in Fig. 1a is $d = (21.0 \pm 0.2)$ Å. The tilt angle of the molecules away from the layers' normal is then $\alpha = \arccos(d/l) = (28 \pm 1)^\circ$. The tilt implies that the neighboring molecules are shifted with respect to each other, by $\arcsin(d/l) \approx (2.3 \pm 0.2)$ Å. The DIO monolayer structure in Fig. 1a,b remains the same when the preparation temperature varies in the range (20 – 80)°C. Remarkably, the STM images show no molecular dimerization or overlapping.

To quantify the contrasts in the STM images, quantum-chemical calculations are performed for a neutral isolated DIO molecule (Supplemental Material [31], see also references [2,32–34] therein). The calculations show that estimated length and width of the backbone and the shapes of frontier molecular wavefunctions defined by a π -conjugated core of the molecule are in good agreement with the bright regions in STM images, Fig. 1b. The distribution of contrasts confirms the polar orientational order of ferroelectric molecules as depicted in Fig. 1c: the DIO electric dipoles (~ 9.43 D [2]) point in the same direction.

The observed polar ordering of DIO molecules differs drastically from arrangements in monolayers of conventional liquid crystals, such as cyanobiphenyls [35,36] and antiferroelectric smectics [37,38], in which the electric dipoles of

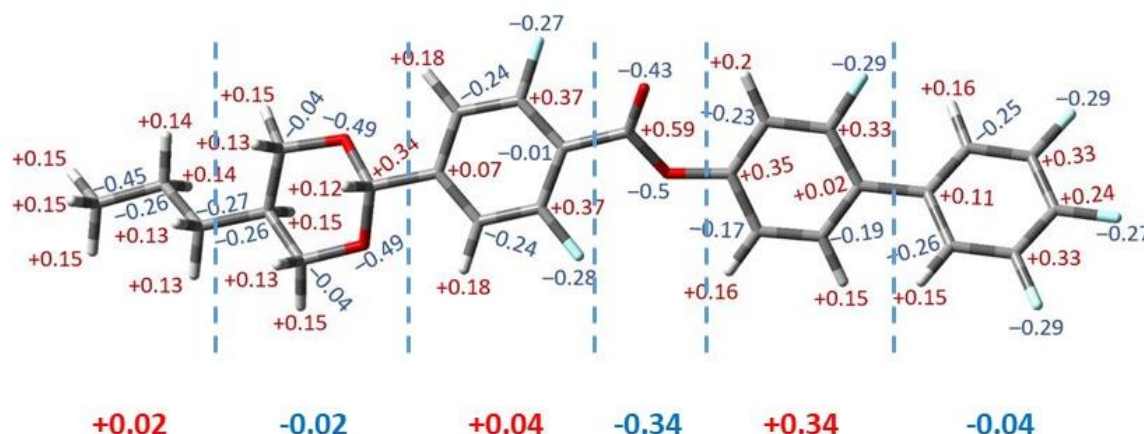
neighboring molecules are antiparallel. To further demonstrate the difference, we explored monolayers of 4,4'-n-decyl-cyanobiphenyl (10CB) at the same Au(111) substrates. In its bulk form, 10CB shows a direct transition from the isotropic to the smectic-A phase, Iso – 50.2 °C – SmA – 44 °C – Cr. The STM textures reveal head-to-head pairing of molecules, Fig. 1d, with their dipoles **D**, on the order of 6 Debye, being antiparallel. This result is in line with other STM observations of apolar orientations in monolayers of molecules which form apolar bulk LC phases [35,36,39-46].

The smectic C-like polar structure in Fig.1b,c is different from the bulk 3D arrangements of DIO, which form the paraelectric N, antiferroelectric SmZ_A and ferroelectric N_F phases [2,7]. The observed polar order and shifts along the polar axis cannot be explained by a simple model of point-like dipoles. Instead, the data provide support for the model of longitudinal surface charge density wave proposed by Madhusudana [47]. The N_F molecules are modeled as cylindrical rods with a chain of alternating positive and negative electric charges along the long axes. A shift of one molecule with respect to its side neighbor by half-period ζ of the charged wave produces strong electrostatic attraction of two molecules oriented in a syn-polar fashion. This polar arrangement is of a lower electrostatic energy than the antiparallel assembly when the distances between the molecules are short [47]. As the separations increase, the contributions from different charges overlap and an antiparallel arrangement prevails.

Figure 2a presents the static site charge distribution of a DIO molecule, calculated by DFT with the hybrid B3LYP functional and the split valence basis set 6-31G* using the Gaussian'03 package [34]. The molecule can be conditionally split into parts along its length, with the charges summed up within each part. One possible summation scheme with six parts is shown in Fig. 2a. The wave of alternating positive and negative charges is similar to the Madhusudana's model [47]. Therefore, the shift of a DIO molecule with respect to its neighbor can result from the electrostatic attraction of oppositely charged groups of the two molecules, as schematized in Fig. 2b. An important condition of the model [47] is that the end charges are relatively

weak, which is the case of the DIO molecule, one end of which contains three fluorine substitutions in ortho positions and the other end is a short aliphatic chain, Fig. 2.

a



b

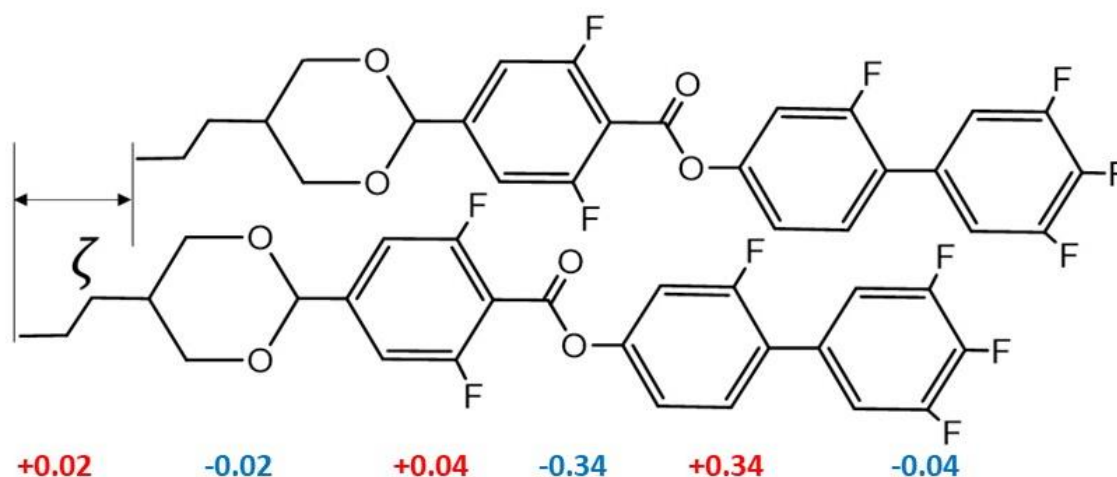


Figure 2. DIO molecules: (a) electric charge distribution evaluated using the Gaussian'03 package; red and blue are positive and negative charges, respectively; (b) scheme of the electric charge longitudinal wave and shifts of DIO molecules providing side-by-side attractions of the molecules in syn-polar orientation.

Conclusion

We presented the first direct observation of polar molecular ordering in the monolayer of ferroelectric nematic mesogens, which is in strike contrast to the behavior of conventional nematics. Molecules of conventional nematics adsorbed on atomically flat crystal surfaces exhibit non-polar ordering, even if they carry a significant electric dipole moment, as in the case of cyanobiphenyls, Fig.1d. The molecules of ferroelectric

nematic DIO, however, adsorbed on a reconstructed Au(111) surface exhibit a high degree of polar ordering, Fig. 1b. The DIO molecules shift with respect to each other along the alignment axis so that the 2D monolayer resembles the smectic C, in which molecules within the layers are tilted. The experiments support the model [47] of ferroelectric nematic ordering in which the syn-polar molecules electrostatically attract each other in side-by-side positions thanks to the wave of alternating positive and negative electric charges along the molecules. Note that the waves of alternating charges along the molecular axes allows electrostatic attraction of similarly charged biomolecules such as nucleic acids in an ionic environment [48].

The polarly ordered N_F monolayers exhibit an extremely thin form factor, which makes them useful for organic microelectronic and nanoelectronic applications. Overall, self-organization is a key process in many scientific and technological fields, and understanding how ferroelectric nematic molecules organize themselves on surfaces is essential for advancing general knowledge and developing new materials.

Acknowledgments

The quantum-chemical calculations were run on the computer cluster at Bogolyubov Institute for Theoretical Physics of NASU. This work was supported by NASU projects No. 0121U109816, 0123U100832; the Long-term program of support of the Ukrainian research teams at the PAS Polish Academy of Sciences carried out in collaboration with the U.S. National Academy of Sciences with the financial support of external partners via the agreement No. PAN.BFB.S.BWZ.356.022.2023; the NATO Science for Peace and Security Programme grant SPS G6030; Kent State University's Ukraine Scholars Fund. ODL acknowledges the support of NSF grant ECCS-2122399. YYL acknowledges the European fund for displaced scientists (EFDS program from ALLEA and Breakthrough Prize Foundation) and MSCA4Ukraine fellowship scheme (No. 1232376), which is funded by the European Union.

References

- [1] P. G. de Gennes and J. Prost, *The Physics of Liquid Crystals* (Clarendon Press, Oxford, 1993).
- [2] H. Nishikawa, K. Shiroshita, H. Higuchi, Y. Okumura, Y. Haseba, S. I. Yamamoto, K. Sago, and H. Kikuchi, *A Fluid Liquid-Crystal Material with Highly Polar Order*, *Adv Mater* **29**, 1702354 (2017).
- [3] R. J. Mandle, S. J. Cowling, and J. W. Goodby, *A nematic to nematic transformation exhibited by a rod-like liquid crystal*, *Phys Chem Chem Phys* **19**, 11429 (2017).
- [4] A. Mertelj, L. Cmok, N. Sebastián, R. J. Mandle, R. R. Parker, A. C. Whitwood, J. W. Goodby, and M. Čopič, *Splay Nematic Phase*, *Phys Rev X* **8**, 041025 (2018).
- [5] N. Sebastián, L. Cmok, R. J. Mandle, M. R. de la Fuente, I. D. Olenik, M. Čopič, and A. Mertelj, *Ferroelectric-Ferroelastic Phase Transition in a Nematic Liquid Crystal*, *Phys Rev Lett* **124**, 037801 (2020).
- [6] X. Chen *et al.*, *First -principles experimental demonstration of ferroelectricity in a thermotropic nematic liquid crystal: Polar domains and striking electro-optics*, *Proceedings of the National Academy of Sciences of the United States of America* **117**, 14021 (2020).
- [7] X. Chen *et al.*, *The smectic ZA phase: Antiferroelectric smectic order as a prelude to the ferroelectric nematic*, *Proceedings of the National Academy of Sciences of the United States of America* **120**, e2217150120 (2023).
- [8] H. Kikuchi, H. Matsukizono, K. Iwamatsu, S. Endo, S. Anan, and Y. Okumura, *Fluid Layered Ferroelectrics with Global $C_{\infty v}$ Symmetry*, *Adv Sci* **9**, 2202048 (2022).
- [9] X. Chen *et al.*, *Observation of a uniaxial ferroelectric smectic A phase*, *Proceedings of the National Academy of Sciences of the United States of America* **119**, e2210062119 (2022).
- [10] X. Chen, E. Korblova, M. A. Glaser, J. E. Maclennan, D. M. Walba, and N. A. Clark, *Polar in-plane surface orientation of a ferroelectric nematic liquid crystal:*

- Polar monodomains and twisted state electro-optics*, Proceedings of the National Academy of Sciences of the United States of America **118**, e2104092118 (2021).
- [11] F. Caimi, G. Nava, R. Barboza, N. A. Clark, E. Korblova, D. M. Walba, T. Bellini, and L. Lucchetti, *Surface alignment of ferroelectric nematic liquid crystals*, Soft Matter **17**, 8130 (2021).
- [12] D.-K. Yang and S.-T. Wu, *Fundamentals of Liquid Crystal Devices* (John Wiley & Sons, Chichester, England, 2006).
- [13] J. X. Li *et al.*, *Development of ferroelectric nematic fluids with giant-epsilon dielectricity and nonlinear optical properties*, Science Advances **7**, eabf5047 (2021).
- [14] P. Rudquist, *Revealing the polar nature of a ferroelectric nematic by means of circular alignment*, Sci Rep-Uk **11**, 24411 (2021).
- [15] S. Brown, E. Cruickshank, J. M. D. Storey, C. T. Imrie, D. Pocięcha, M. Majewska, A. Makal, and E. Gorecka, *Multiple Polar and Non-polar Nematic Phases*, Chemphyschem **22**, 2506 (2021).
- [16] N. Sebastián, R. J. Mandle, A. Petelin, A. Eremin, and A. Mertelj, *Electrooptics of mm-scale polar domains in the ferroelectric nematic phase*, Liq Cryst **48**, 2055 (2021).
- [17] X. Chen, Z. C. Zhu, M. J. Magrini, E. Korblova, C. S. Park, M. A. Glaser, J. E. Maclennan, D. M. Walba, and N. A. Clark, *Ideal mixing of paraelectric and ferroelectric nematic phases in liquid crystals of distinct molecular species*, Liq Cryst **49**, 1531 (2022).
- [18] B. Basnet, M. Rajabi, H. Wang, P. Kumari, K. Thapa, S. Paul, M. O. Lavrentovich, and O. D. Lavrentovich, *Soliton walls paired by polar surface interactions in a ferroelectric nematic liquid crystal*, Nature Communications **13**, 3932 (2022).
- [19] N. Sebastián, M. Čopič, and A. Mertelj, *Ferroelectric nematic liquid-crystalline phases*, Phys Rev E **106**, 27, 021001 (2022).
- [20] H. Nishikawa, K. Sano, S. Kurihara, G. Watanabe, A. Nihonyanagi, B. Dhara, and F. Araoka, *Nano-clustering mediates phase transitions in a diastereomerically-stabilized ferroelectric nematic system*, Commun. Mater. **3**, 89 (2022).

- [21] J. S. Yu, J. H. Lee, J. Y. Lee, and J. H. Kim, *Alignment properties of a ferroelectric nematic liquid crystal on the rubbed substrates*, *Soft Matter* **19**, 2446 (2023).
- [22] R. Barboza *et al.*, *Explosive electrostatic instability of ferroelectric liquid droplets on ferroelectric solid surfaces*, *Proceedings of the National Academy of Sciences of the United States of America* **119**, 7, e2207858119 (2022).
- [23] L. Cmok, V. Coda-Bouchot, N. Sebastian, A. Mertelj, M. Zgonik, S. Aya, M. J. Huang, G. Montemezzani, and I. Drevenšek-Olenik, *Running streams of a ferroelectric nematic liquid crystal on a lithium niobate surface*, *Liq Cryst* **50**, 1478 (2023).
- [24] A. Sterle, L. Cmok, N. Sebastian, A. Mertelj, Y. F. Kong, X. Z. Zhang, and I. Drevenšek-Olenik, *Light-induced dynamics of liquid-crystalline droplets on the surface of iron-doped lithium niobate crystals*, *Opt Mater Express* **13**, 282 (2023).
- [25] S. Marni, G. Nava, R. Barboza, T. G. Bellini, and L. Lucchetti, *Walking Ferroelectric Liquid Droplets with Light*, *Adv Mater* **35**, 2212067 (2023).
- [26] F. Caimi, G. Nava, S. Fuschetto, L. Lucchetti, P. Paiè, R. Osellame, X. Chen, N. A. Clark, M. A. Glaser, T. Bellini, *Fluid superscreening and polarization following in confined ferroelectric nematics*, *Nat Phys* **19**, 1658 (2023).
- [27] F. Hanke and J. Björk, *Structure and local reactivity of the Au(111) surface reconstruction*, *Phys Rev B* **87**, 235422 (2013).
- [28] J. V. Barth, H. Brune, G. Ertl, and R. J. Behm, *Scanning Tunneling Microscopy Observations on the Reconstructed Au(111) Surface - Atomic-Structure, Long-Range Superstructure, Rotational Domains, and Surface-Defects*, *Phys Rev B* **42**, 9307 (1990).
- [29] D. P. E. Smith, J. K. H. Horber, G. Binnig, and H. Nejh, *Structure, Registry and Imaging Mechanism of Alkylcyanobiphenyl Molecules by Tunneling Microscopy*, *Nature* **344**, 641 (1990).
- [30] A. J. Fisher and P. E. Blochl, *Adsorption and Scanning-Tunneling-Microscope Imaging of Benzene on Graphite and Mos₂*, *Phys Rev Lett* **70**, 3263 (1993).
- [31] See Supplemental Material [url] for quantum-chemical calculations for a DIO molecule, which includes Refs. [32-34].

- [32] A. D. Becke, *Density-Functional Thermochemistry. III. The Role of Exact Exchange*, J Chem Phys **98**, 5648 (1993).
- [33] C. T. Lee, W. T. Yang, and R. G. Parr, *Development of the Colle-Salvetti Correlation-Energy Formula into a Functional of the Electron-Density*, Phys Rev B **37**, 785 (1988).
- [34] M. J. Frisch *et al.*, *Gaussian 03, Revision B.05* (Gaussian Inc., Pittsburgh, PA, 2003).
- [35] Y. Iwakabe, M. Hara, K. Kondo, K. Tochigi, A. Mukoh, A. Yamada, A. F. Garito, and H. Sasabe, *Correlation between Bulk Orderings and Anchoring Structures of Liquid-Crystals Studied by Scanning Tunneling Microscopy*, Jpn J Appl Phys 1 **30**, 2542 (1991).
- [36] J. Noh, T. Murase, K. Nakajima, H. Lee, and M. Hara, *Nanoscopic investigation of the self-assembly processes of dialkyl disulfides and dialkyl sulfides on Au(111)*, Journal of Physical Chemistry B **104**, 7411 (2000).
- [37] M. Hara, T. Umemoto, H. Takezoe, A. F. Garito, and H. Sasabe, *Novel Quadruple Zigzag Structure of Antiferroelectric Liquid-Crystal Molecules Observed by Scanning Tunneling Microscopy*, Japanese Journal of Applied Physics Part 2-Letters & Express Letters **30**, L2052 (1991).
- [38] K. D. Jandt, S. Tixier, M. J. Towler, J. M. Blackmore, and M. J. Miles, *Observation of Phase-Transitions in an Antiferroelectric Liquid-Crystal Investigated by Scanning-Tunneling-Microscopy*, J Appl Phys **77**, 122 (1995).
- [39] J. S. Foster and J. E. Frommer, *Imaging of Liquid-Crystals Using a Tunnelling Microscope*, Nature **333**, 542 (1988).
- [40] K. Walzer and M. Hietschold, *Comparative scanning tunneling microscopy observation of a homologous series of n-alkyloxy-cyanobiphenyles*, J Vac Sci Technol B **14**, 1461 (1996).
- [41] D. P. E. Smith, W. M. Heckl, and H. A. Klagges, *Ordering of Alkylcyanobiphenyl Molecules at Mos2 and Graphite Surfaces Studied by Tunneling Microscopy*, Surface Science **278**, 166 (1992).

- [42] S. L. Brandow, D. P. Dilella, R. J. Colton, and R. Shashidhar, *Evidence of Pronounced Positional Order at the Graphite Liquid-Crystal Interface of a Bulk Nematic Material*, *J Vac Sci Technol B* **9**, 1115 (1991).
- [43] J. P. Michel, E. Lacaze, M. Alba, M. Goldmann, and F. Rieutord, *Physisorption of 4-octyl-4'-cyanobiphenyl (8CB) molecules on MoS₂: interpretation of pairing phenomenon*, *Surface Science* **507**, 374 (2002).
- [44] J. K. Spong, L. J. Lacombe, M. M. Dovek, J. E. Frommer, and J. S. Foster, *Imaging of Liquid-Crystals with Tunneling Microscopy*, *J Phys-Paris* **50**, 2139 (1989).
- [45] D. L. Patrick and T. P. Beebe, *Substrate Defects and Variations in Interfacial Ordering of Monolayer Molecular Films on Graphite*, *Langmuir* **10**, 298 (1994).
- [46] S. V. Snegir, O. L. Kapitanchuk, E. Lacaze, and A. Marchenko, *STM Study of Self-Organization of 10CB Molecules on Au(111) Surface*, *Mol Cryst Liq Cryst* **589**, 90 (2014).
- [47] N. V. Madhusudana, *Simple molecular model for ferroelectric nematic liquid crystals exhibited by small rodlike mesogens*, *Phys Rev E* **104**, 014704 (2021).
- [48] J. Lipfert, S. Doniach, R. Das, and D. Herschlag, *Understanding Nucleic Acid-Ion Interactions*, *Annu Rev Biochem* **83**, 813 (2014).

SUPPLEMENTARY INFORMATION

To quantify the contrasts in the STM images, quantum-chemical calculations are performed for a neutral isolated DIO molecule. The geometry optimization and electronic structure calculations are carried out at the density functional theory (DFT) level with the hybrid B3LYP functional [32,33] and the split valence basis set 6-31G* using Gaussian'03 program package [34]. The calculations show that the optimized ground state is the *trans* conformation of the molecular backbone, Fig. S1. The alternative *cis* conformation is not energetically favorable. The *cis*-conformation implies a "bent" shape (almost 90 degrees), which is not observed in the STM experiment. The calculated dipole of the DIO molecules is 9.42 Debye (9.43 [2]). The estimated length and width of the backbone and the shapes of frontier molecular wavefunctions defined by a π -conjugated core of the molecule are in good agreement with the bright contrast regions in STM images, Fig. 1b. Since the calculated HOMO-LUMO gap for the DIO molecule exceeds 4eV, which is substantially larger than the applied bias tunneling voltages (50-500mV), there is no dependence of STM contrast on the applied voltage. The distribution of contrasts observed in the STM image suggests the polar orientational order of ferronematic molecules at the Au(111) substrate as depicted in Fig. 1c: permanent electric dipoles of neighboring molecules are pointed in the same direction giving rise to the SAM with a polar ordering.

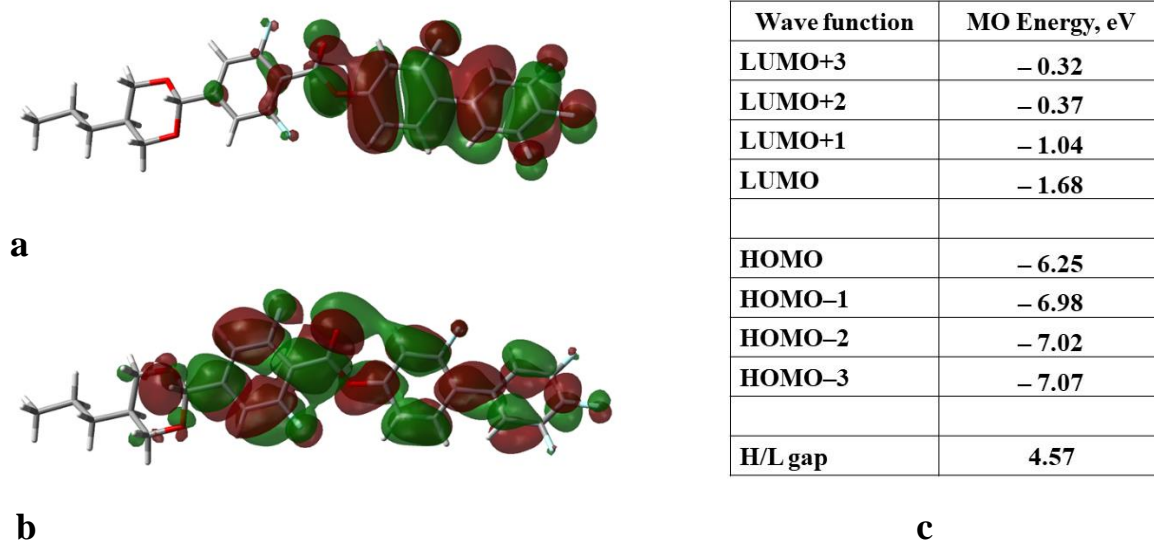


Figure S1. The profiles of calculated (a) HOMO (-6.25 eV) and (b) LUMO (-1.68 eV) wavefunctions in the neutral ground state of the molecule. Different colors of the molecular orbital surfaces represent a phase of the wave functions (red for

positive, green for negative). (c) The energies of four frontier HOMO and LUMO levels for neutral molecules in the gas phase.